Parasitology Research (2025) 124:30
https://doi.org/10.1007/s00436-025-08466-4

RESEARCH

Immunolocalization and 3D modeling of three unique proteins belonging to the costa of *Tritrichomonas foetus*

Paula Terra Bandeira[1] · Camila Rodrigues Chaves[2] · Pedro Henrique Monteiro Torres[2] · Wanderley de Souza[1,3]

Received: 27 September 2024 / Accepted: 10 February 2025 / Published online: 7 March 2025

Abstract

Nowadays, even in light of all the massive advances in cell biology, we still find some cellular structures that are not entirely understood. Among those, we highlight the costa, a structure from the mastigont system existent only in some members of the orders Trichomonadida and Tritrichomonadida, including the pathogens of venereal diseases in humans and cattle, *Trichomonas vaginalis* (*T. vaginalis*) and *Tritrichomonas foetus* (*T. foetus*), respectively. The costa is a prominent striated fiber and, although part of the cytoskeleton, differs from its classical components, and its molecular composition is still not fully characterized. Using proteomics of *T. foetus*'s costa fraction, we previously identified hypothetic proteins, and among these, the protein ARM19800.1 positively localized in the costa and named costain-1. In this study, two other protein candidates were analyzed. To achieve the specific localization of 11810 and 32137 proteins in *T. foetus*'s cells, it was used expansion microscopy and immunocytochemistry. The immunofluorescence revealed the presence of both proteins throughout the whole costa but with different intensities. Immunocytochemistry using negative staining, LR-White, and Epon embedding revealed further analyses of the protein's localization. All techniques confirmed the distinct and distributed localization of both proteins: costain-2 (11810) and costain-3 (32137). Also, AlfaFold3 was used to generate 3D models of the three identified proteins, showing a major prevalence of α-helical spans. Nonetheless, the identification and further characterization of these unique proteins can help understand their functional role in the assembled costa and, therefore, better understand the organization and function of this structure in these organisms.

Keywords Costa · Costain · Cytoskeleton · Immunolocalization · *Tritrichomonas foetus* · AlphaFold3

Introduction

Trichomonads are a group of unicellular eukaryotic organisms, including free-living, symbiotic, and parasitic species. Trichomonads that act as parasites or opportunistic pathogens can cause diseases such as trichomoniasis, leading to widespread dissemination and significant economic and social impacts, which remain underappreciated (Bassey et al. 2022; Beatty et al. 2022; Eslahi et al. 2021; Matthew et al. 2023; Meites 2013; Muzny 2018; Secor et al. 2014). Therefore, further investigation of these unicellular eukaryotes is essential for a deeper understanding of their biology and life cycle. Such findings can reveal potential new drug targets and antigens that can be used to treat these diseases or elaborate new vaccines to prevent these infections.

Furthermore, due to its early localization in the eukaryotic branch of evolution, these cells can be used as an interesting model for studying general and specific eukaryotic features (Archibald 2015). Among these features, we can

Section Editor: Luiz Claudio Miletti

✉ Paula Terra Bandeira
paulaterrabandeira@gmail.com

[1] Laboratório de Ultraestrutura Celular Hertha Meyer, Centro de Pesquisa Em Medicina de Precisão, Instituto de Biofísica Carlos Chagas Filho, Universidade Federal Do Rio de Janeiro, Rio de Janeiro, Brazil

[2] Laboratório de Modelagem E Dinâmica Molecular, Instituto de Biofísica Carlos Chagas Filho, Universidade Federal Do Rio de Janeiro, Rio de Janeiro, Brazil

[3] Instituto Nacional de Ciência E Tecnologia Em Biologia Estrutural E Bioimagens, and Centro Nacional de Biologia Estrutural E Bioimagens, Universidade Federal Do Rio de Janeiro, Rio de Janeiro, Brazil

highlight the absence of mitochondria and the presence of hydrogenosomes, which have different mechanisms for anaerobic ATP synthesis, and also the presence of a mastigont system, which comprises some common cytoskeleton structures along with some unique arrangements or elements, like the parabasal and sigmoid filaments, the pelta-axostyle system, and the costa (Benchimol 2010).

The costa is a part of the cytoskeleton of the trichomonads that possess an undulating membrane. It is a large cell structure that displays an intricate birefringent pattern like a striated root in a rod-shaped format. It may reach a length of 14.38 ± 1.3 µm and a width of 36.5 ± 3.4 nm. It is also striated, having alternating electron-lucent and electron-dense bands of $13.8 + 1.25$ nm and 241.3 ± 13.9 nm in length, respectively. Through electron microscopy tomography analysis, it was possible to note that the electron-lucent bands are not uniform and display a small amorphous region in the inner portion of the costa; on the other hand, the dense bands were homogeneous (Benchimol 2010).

The costa emerges from the region of the R kinetosome and Basal Body 1 and 3, and it goes throughout the cell continuously underneath the undulating membrane and the recurrent flagellum (de Andrade Rosa et al. 2017). Because of this, it is hypothesized that it has the function to dissipate the mechanical stress from the beating of the recurrent flagellum. Initial studies on the chemical composition of the costa suggested that it was mainly composed of carbohydrates (Sledge et al. 1978). However, electron microscopy cytochemical studies showed that the costa is mainly composed of proteins, especially basic ones (Amos et al. 1979; Benchimol et al. 1982; de Andrade Rosa et al. 2017). Subsequent isolation of the structure confirmed the presence of proteins (Amos et al. 1979; de Andrade Rosa et al. 2017; Monteiro-Leal et al. 1993; Viscogliosi and Brugerolle 1994, 1993).

In previous studies from our group, using proteomic analysis of enriched costa fractions, we identified 44 hypothetical proteins without conserved domains (de Andrade Rosa et al. 2017). The protein that was present at the highest concentration in the proteomic analysis, protein 8327 (PubMed: ARM19800.1), was selected for the production of specific polyclonal antibodies to proceed with its immunolocalization in isolated costa. After confirmation as the first identified protein from the costa of *T. foetus*, it was named costain-1 (Bandeira and de Souza 2022). Using immunofluorescence and transmission electron microscopy of an enriched costa fraction, it was possible to confirm the distribution of the costain-1 throughout the whole costa. The use of expansion microscopy made it possible to obtain a more detailed view of the costain-1 localization in whole *T. foetus* cells (Bandeira et al. 2023).

In the present study, we continue to identify and characterize costa proteins. Thus, we selected two of the most concentrated ones in the proteomic analyses, protein 11810 and protein 32137, for further analysis. Here, we report the localization and identification of two new costa proteins through immune assays using fluorescence and electron microscopy, and also a comparative modeling methodology was used to generate 3D models of the three identified costa proteins in search of a deeper understanding of them.

Materials and methods

Protozoan maintenance

We used the K strain of *T. foetus* isolated from the urogenital tract of a bull (Embrapa, Rio de Janeiro, Brazil). The parasite was cultivated in Diamond's trypticase yeast-extract maltose medium (TYM; Diamond 1957) supplemented with 10% fetal bovine serum, and the cells were grown for 24 h at 37 °C.

Antibodies

We used a monoclonal anti-α tubulin antibody (Sigma-Aldrich, Clone B512) at a 1:400 dilution for tubulin labeling. For the costa labeling, it was used the already tested anti-costain-1 (Bandeira and de Souza 2022) and the two new antibodies, designed based on protein candidates previously selected due to the proteomic analysis of the costa. The first candidate was the 11810 protein (EKVKLQSKAQLDAIYDQLEK peptide from the sequence ARM19816.1—accession in GenBank), and the other was the 32137 protein (DKARETITKLSKSDLAIRR peptide from the sequence ARM19912.1—accession in GenBank). These peptides were selected among the most antigenic ones after the LifeTein antigenic analysis, chemically synthesized, and used for rabbit immunization (LifeTein, South Plainfield, NJ 07080, USA). For the Western blot analysis, we used 1:1000 dilution; for the immunostaining, various dilutions were tested and the 1:100 dilution was the chosen one. The secondary antibodies were Alexa Fluor 488-conjugated anti-rabbit IgG antibody and Alexa Fluor 546-conjugated anti-mouse IgG antibody (Life Technologies) for the immunofluorescence assays and goat anti-rabbit conjugated to 5 or 10 nm gold particles (Ted Pella; Redding, CA) for transmission electron microscopy (TEM) assays.

Western blot

The total protein extract from *T. foetus* cells, the enriched costa fraction (ECF), and a partial purification between both samples were all individually (20 µg each) mixed with the sample buffer, boiled, and applied in three SDS-PAGE 8% gradient gels (Laemmli 1970) along with the Kaleidoscope

Prestained Standard (Bio-Rad, Brazil) as a protein standard. One gel was stained with Coomassie Brilliant Blue G-250, and the other two were used for testing the new antibodies. The proteins were transferred from the gel to a nitrocellulose membrane (ECL-Hybond, Amersham) using the semi-dry method (Trans-blot SD, BioRad) and then blocked in a 5% non-fat milk in TBST (20 mmol/L Tris base, pH 8.0, 150 mM NaCl, 0.5% Tween-20). Next, they were incubated overnight on a shaker with each primary antibody (anti-32137 or anti-11810 at 1:1000 dilution) in its respective membrane. The membranes were washed and incubated with a secondary antibody (HRP goat anti-rabbit Ig), and the chemiluminescent signal was acquired using Clarity Western ECL Substrate (BioRad) and ImageQuant LAS500 (GE Healthcare).

Immunolocalization

For the immunolocalization of the two new costa protein candidates, whole cell lysates or the ECF was used, as previously described (Bandeira and de Souza 2022; de Andrade Rosa et al. 2017). Then, we tried different microscope techniques to localize each protein, as described below.

Expansion microscopy and immunofluorescence

Since our previous work showed that using expansion microscopy (ExM) intensified and allowed the best immunolabeling of the costa inside the cell, we also used the same approach for this study (Bandeira et al. 2023). Briefly, the cells were adhered to glass coverslips previously coated with poly-D-lysine for 10 min at room temperature (RT). Next, the coverslips were submersed in a 2 × 0.7% AA/1% FA mix at 37 °C for 5 h using 12 wells plates. For the gelation step, it was used APS and Temed along with the monomer solution (19% sodium acrylate; 10% AA; 0.1% BIS-AA in PBS 10X) at 37 °C for 1 h for polymerization of the gels containing the samples. Then, the proteins were denatured by incubation at 95 °C for 1:30 h. Afterwards, the gels were incubated in water 3 times and then overnight. The next day, for the immunostaining, the gels were allowed to shrinkage in PBS (3 times, 10 min each). Then, the gels were incubated with each one of the three antibodies individually: anti-costain-1, anti-32137, or anti-11810 at 1:100 dilution each. Whole cells were also labeled with anti-α-tubulin (1:400) for 3 h at 37 °C. After rinsing in PBS-Tween 0.1% (3 times), the samples were incubated sequentially with the respective secondary antibodies, anti-rabbit Alexa Fluor 488 and anti-mouse Alexa Fluor 546 (1:500 in PBS) in the same conditions. Finally, the gels were washed again in PBS-Tween 0.1% (3 times) and proceeded with the second round of expansion in water (3 times for 30 min and then overnight) (Bandeira et al. 2023; Dos Santos Pacheco and Soldati-Favre 2021). The next day, the gels were observed in an inverted microscope, both in the Axio Observer or the Elyra PS.1 microscope (Carl Zeiss Meditec AG, Jena, Germany) equipped with ZEN 2012 software (version 9.1.1.5), and the images were processed using ZEN software (Carl Zeiss Meditec AG, Jena, Germany).

Transmission electron microscopy

Negative staining The ECF was allowed to adhere to glow-discharged and formvar-coated grids for negative staining. The grids were then rinsed in PEME buffer (100 mM PIPES, 1 mM MgSO4, 0.1 mM EDTA, and 2 mM EGTA, pH 6.9) for 5 min and fixed in 4% freshly prepared formaldehyde plus 0.1% glutaraldehyde in PEME for 10 min. Next, the grids were incubated on droplets of diluent (PBS-1% BSA) for 30 min and then transferred to droplets of the primary antibody (costain-1, anti-32137 or anti-11810 or PBS + 1%BSA as negative control). Several dilutions were tested (1:100, 1:1000, and 1:10.000) at 1-h incubation. The grids were then rinsed 3 times for 5 min each and transferred to droplets of species-specific secondary antibodies: goat anti-rabbit conjugated to 5 or 10 nm gold (Ted Pella; Redding, CA) diluted 1:50 and incubated for 1 h. The grids were then rinsed 3 times in PBS for 5 min each and finally with distilled water. The grids were then fixed in 2.5% (v/v) glutaraldehyde in PEME for 10 min and subsequently negatively stained with 1% (v/v) aurothioglucose in water (adapted from Vidal et al. 2016).

Hydrophilic resin immunostaining (LR-White) The *T. foetus* cells were initially fixed in a solution containing 4% freshly prepared formaldehyde and 0.1% glutaraldehyde solution for 1 h at 4 °C, dehydrated with ethanol, and infiltrated in LR-White resin. Afterwards, the grids were incubated as described above in the "Negative staining" section for the immunostaining, dried, and observed in transmission electron microscope.

Epon immunostaining The *T. foetus* cells were fixed with 2.5% glutaraldehyde in 0.1 M cacodylate buffer, pH 7.2, washed in PBS, and postfixed in 1% OsO4 containing 0.8% potassium ferrocyanide in 0.1 M cacodylate buffer, pH 7.2. Then, it was washed in PBS, dehydrated in acetone, and embedded in Epon. Then, the sections were exposed to a pre-treatment with 0.3% hydrogen peroxide to help increase immunoreactivity by reducing osmification of the target molecules. Immunolabeling was made as described in the "Negative staining" section. Ultrathin sections were stained with uranyl acetate and lead citrate and observed in transmission electron microscope.

Imaging Observations of each technique were made in a Hitachi HT 7800 or FEI Tecnai T20 transmission electron microscopes, operating at 100 kV or 200 kV, respectively, and images were acquired.

Sequence and structure characterization

Sequences were retrieved from GenBank accessions ARM19800.1 (costain-1), ARM19816.1 (costain-2), and ARM19912.1 (costain-3). All sequences were subject to a multiple sequence alignment using Kalign (Lassmann 2020) through Ugene software (Okonechnikov et al. 2012), which was also used to generate an identity matrix. Sequences were submitted to SMART server (Letunic et al. 2021), InterPro (Paysan-Lafosse et al. 2023), and CD-Search (Wang et al. 2023) for domain identification. Subsequently, all proteins were modeled with AlphaFold3 Server (Abramson et al. 2024) in order to generate a representative 3D structure, and the quality of the models is estimated through the pTM scores (Xu and Zhang 2010; Zhang and Skolnick 2004).

Results and discussion

Western blot

Western blot analysis was carried out for each of the antibodies using the protein content of whole cells, an intermediate fraction, and an enriched costa fraction (EFC) (Fig. 1). The results confirmed the size of the proteins (116.9 kDa for the 11810 protein and 117.44 kDa for the 32137 protein) and, more importantly, showed increasing intensity of the labeling of the protein from the whole cell towards the EFC. The labeling became more intense as the fraction was gradually more concentrated with the costa proteins, showing that these two proteins, like costain-1, are more prominent in the costa fraction. Another common aspect among the three proteins is their size, which is curiously similar, as costain-1 has 121.6 kDa, in agreement with previous findings that described the costal proteins as being mainly in the 100–150 kDa range (Viscogliosi and Brugerolle 1993). However, the 11810-labeling in the partial cell fraction and in the ECF showed another fainter band close to the stronger band. These two close bands can represent perhaps a protein isoform or, maybe, it can bind and drag in another costa protein, as they share some similar amino acid sequences; however, further analysis should be made to understand that. Still, one of the bands is more prominent than the other, and it presents, in the whole cell sample, as a target preference. For the unedited version of the Western blot images, check Supplementary material (Supplementary Fig. 1 and 2).

One of the first attempts to try to identify the costa proteins was made by Viscogliosi and Brugerolle (1993, 1994), when they utilized an SDS-PAGE approach. They obtained several protein bands associated with the costa, with molecular weights ranging from 100 to 145 kDa. These findings were later confirmed through additional SDS-PAGE analysis and proteomic studies (de Andrade Rosa et al. 2017). These molecular weights are in accordance with the size of costain-1 (Bandeira and de Souza 2022) and the 11810 and 32137 proteins.

Expansion microscopy and immunofluorescence

In the immunolocalization assays, we initially used conventional immunofluorescence microscopy to localize the proteins using the antibodies produced against the protein candidates in both the whole cells and the EFC samples.

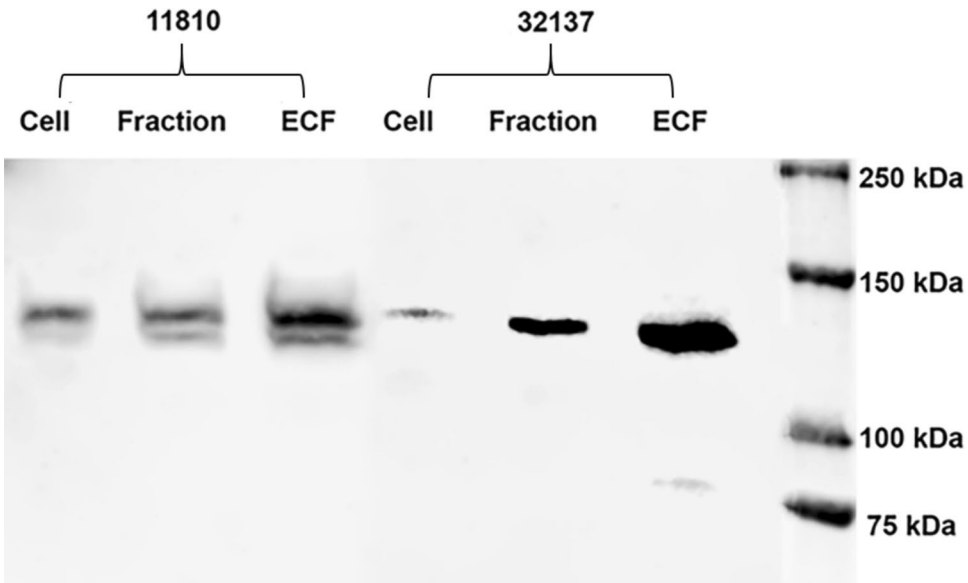

Fig. 1 Western blot analysis of the presence of proteins 11810 (116.9 kDa) and 32137 (117.44 kDa) in the protein content of whole cells, an intermediate cell fraction, and an enriched costa fraction (EFC) showing the gradual enrichment of both proteins in the ECF. Protein ladder is shown in the last lane with the respective kilodaltons (kDa) molecular weights. The results were representative of three biologically independent experiments

However, it was already of our knowledge that the traditional immunofluorescence techniques did not work well for costa staining inside the cell, probably due to the difficulty of reaching the target epitopes. In recent work, our group noted that using expansion microscopy (ExM), it was possible to label the costain-1 in the whole cell, allowing for a better visualization of the costa inside the cell (Supplementary Fig. 5). So, in the present study, we also used the ExM, due to the hypothesis that along with the expansion process, the antigens to which the antibodies bind are more exposed and accessible, making the staining much more effective (Bandeira et al. 2023).

Using the polyclonal antibody made against the protein 11810 in an ExM of *T. foetus* (Fig. 2a, c, d), it is possible to notice a strong positive labeling in green throughout the whole costa, making the 11810 the second confirmed protein of the costa of *T. foetus*. Figure 2b shows a fainter labeling in green, by using the antibody anti-32137. Although the signal is weaker, it is still possible to see the labeling of the costa, confirming the 32137 as the third protein component of the *T. foetus*'s costa. Since both proteins seem to be present in an array of different cell cycles, as shown in Fig. 2a and b, with a variable number of costa per cell, it is also possible to assume that the presence of these proteins is not cell cycle-dependent.

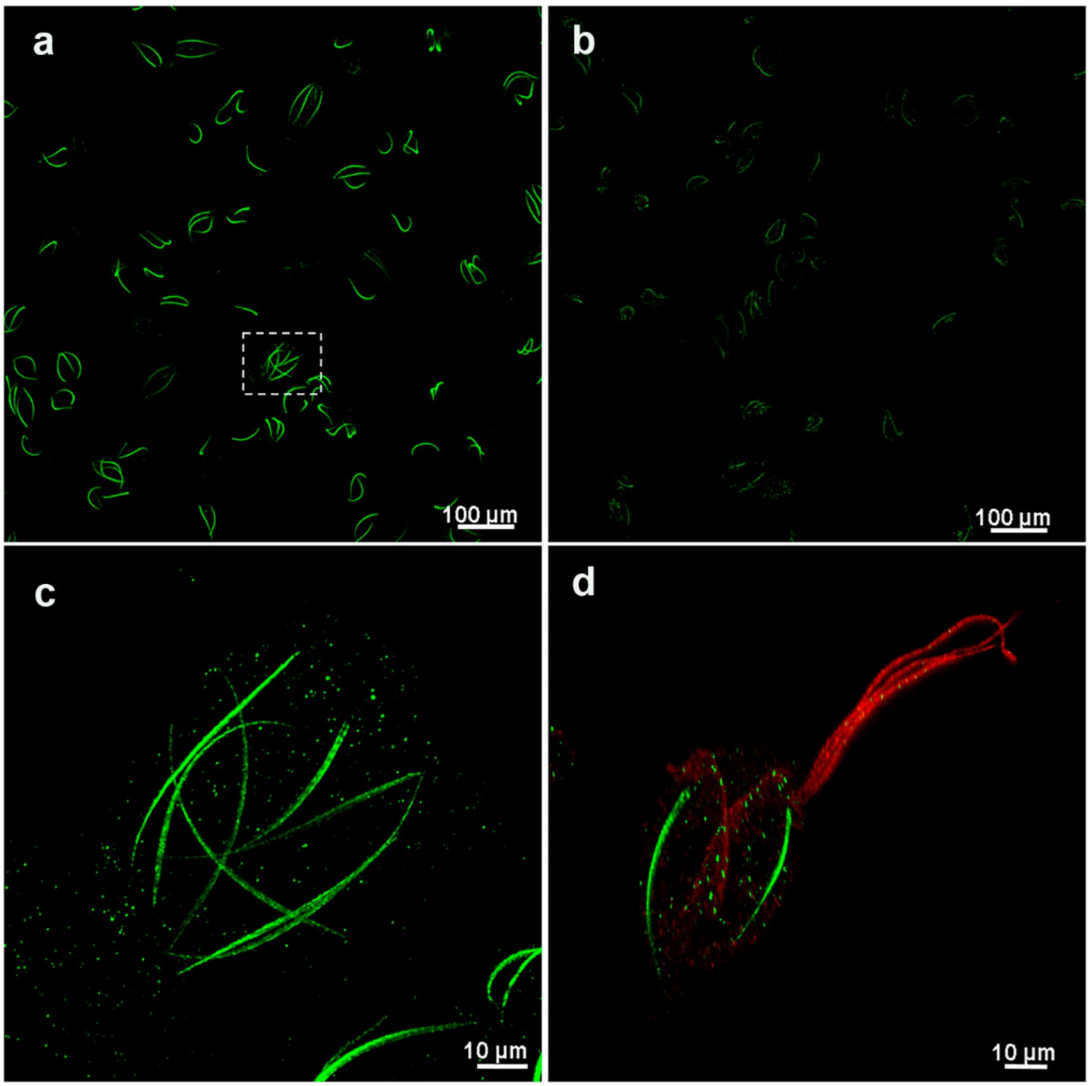

Fig. 2 Expansion microscopy images from *T. foetus*; **a**, **c**, **d** the anti-11810 antibody showed positive labeling in the costa (green). **c** It is possible to see in a more detailed way the cell indicated with a square, showing seven costa in one cell. **d** The anti-α-tubulin antibody (red) was also used, labeling the duplicated axostyle and the flagella in a dividing cell. **b** The anti-32137 antibody was used and also showed positive labeling in the *T. foetus* costa, although in a fainter way than the 11810 labeling. Images obtained in confocal mode on Elyra PS.1 microscope. The results were representative of at least three biologically independent experiments

Interestingly, especially while using a lower amplification scale of the ExM and the labeling of the costa (Fig. 2a, b), it is possible to observe the costa in a much more complex scenario while they are still inside the cells, displaying a variety of shapes, showing how flexible and versatile the costa can be inside the cell. When using only the EFC, this great diversity of shapes is lost, and outside the cell, almost all costa presents the same "smiley-shaped" format. Furthermore, as seen in Fig. 2, when observing the costa in the whole cell, it is possible to notice that many cells display more than one costa. A lot of these cells seem to be in the process of division, especially when the α-tubulin (red) is also labeled, revealing the duplication of the costa (green) and the axostyle (red) (Fig. 2d). Also, in Fig. 2d, it is possible to note that the two costa seem to have different lengths, maybe because of the angle of the image or maybe because the new costa is still in a growing process, and until now, this process is not fully clarified.

Notwithstanding, some cells present more than two costa, displaying even three or four costa, and one cell even displays seven costa, which can be seen in a more detailed way in Fig. 2c, making this cell probably a pseudocyst, a form that *T. foetus* cells assume in certain conditions, where it internalizes the flagella and have multiple nuclei. The pseudocysts are understood as a resistant form to adverse conditions, and it is reversible (Benchimol 2004). However, one recent study showed that multinuclearity is very common in different *T. foetus* and *T. vaginalis* strains in the lab culture (Iriarte et al. 2023).

Unfortunately, the EXM method rarely allows for the acquisition of brightfield images, and we only have the immunofluorescence labeling to guide us. In this case, for a better understanding of the images C and D showing whole cells containing costa (and not an EFC), we added in the supplementary material an image at the same magnification that also includes labeling for tubulin (axostyle) and the nucleus (Supplementary Fig. 6). Additionally, we included an image showing the EFC after expansion labeled with anti-32137 (Supplementary Fig. 7) and another image of the EFC without the expansion in a brightfield view (Supplementary Fig. 8). This way, it is possible to compare how the costa behaves both inside and outside the cell.

Electron microscopy immunolocalization

Different TEM techniques

Electron microscopy confirmed the protein localization and revealed greater detail (Fig. 3). The first technique used was to embed the cells in a hydrophilic resin (LR-White), which can facilitate antibody penetration in the sample compared to non-hydrophilic resins. As shown in Fig. 3a, the negative control (incubated only with the secondary antibody) was without any labeling in the costa, as opposed to the specific immunolabeling in the images representing, respectively, 32137 (j), 11810 (g), and costain-1 (d) labeling. The labeling between the different proteins in LR-White did not show much difference, so we tried the immunostaining in Epon-embedded cells after a wash with hydrogen peroxide 3% for 5 min. The negative control (b) was without labeling as expected. Still, the immunolabeling for 11810 (h) and 32137 (k) was less intense although specific to the costa, and curiously, the costain-1 had the more intensive labeling in this method, but also with some nonspecific labeling in other places of the cell, although showing a clear preference for the costa. In a third assay, a negative staining of the whole cell was made after using detergent to expose the cytoskeleton. In this experiment, the control was also negative (c), and the 11810 protein (i) showed moderate labeling, consistent with what was observed in the LR-White experiment and the fluorescence images. In the 32137 (l) labeling, there was again a diminished immunolabeling in comparison with the LR-White sample but increased labeling compared to the Epon experiment, and this was consistent with the fainter immunolabeling in the fluorescence in Fig. 2b in comparison with the 11810 in Fig. 2a. The costain-1 still had the more intense immunolabeling, which is expected since it appears to be the most prominent protein in the costa's proteome (de Andrade Rosa et al. 2017).

Light microscopy allows for rapid investigation of cells, particularly when combined with molecular biology tools to manipulate gene expression (such as gene overexpression or knockout) or when using antibodies to specific target proteins. It was through light microscopy that the so-called "paracostal granules" were first identified, now known as hydrogenosomes in trichomonadids. Similarly, metachromatic granules, initially observed in trypanosomatids, were also first identified using light microscopy (de Souza 2024). Despite its lower resolution compared to electron microscopy (EM), the faster and simpler sample preparation and easier accessibility of light microscopy make it an indispensable tool. Particularly with the advent of super-resolution microscopy and the expansion microscopy (ExM) technique, both of which offer improved resolution, light microscopy enables innovative observations of proteins in cells, allowing for dynamic analysis that still is not possible by EM.

However, the resolution provided by EM remains unmatched, offering highly detailed ultrastructural insights, albeit at the cost of a more expensive, complex, and time-consuming approach. Furthermore, EM generates different types of images, presenting only sections of the cell at a time. For now, both light and electron microscopy remain complementary tools in the study of cell organization as exemplified by the costa analysis. When making images of the costa by electron microscopy (EM), it is possible to obtain unparalleled detail for

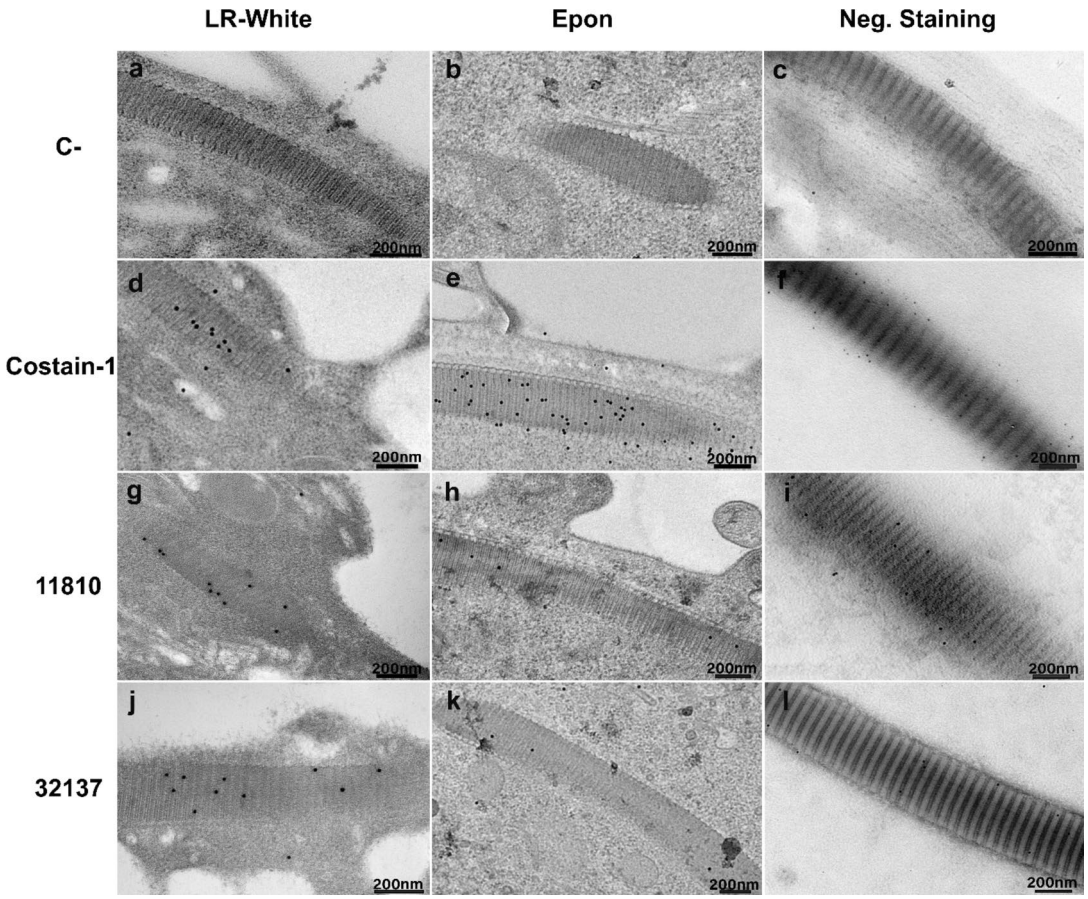

Fig. 3 Immunolabeling using TEM: **a**, **d**, **g**, **j** LR-White embedded *T. foetus* cells. **a** Negative control, **g** anti-11810 antibody, **j** anti-32137 antibody, and **d** anti-costain-1. **b**, **e**, **h**, **k** Have the same labeling order but in Epon treated with 3% hydrogen peroxide. **c**, **f**, **i**–**l** Also have the same labeling order, using negative staining with aurothioglucose after the exposition of the cells with 1% NP-40. The results were representative of at least three biologically independent experiments

ultrastructural studies. However, when analyzing antibody staining to locate proteins, immunofluorescence offers a more comprehensive view of the costa within the cell. In addition to labeling the whole costa, we can now observe a variety of shapes that the costa can adopt inside the cell. It was also possible to clearly identify that a few cells display more than two costa, which is not usual. These diverse shapes highlight the costa as a stable yet highly flexible structure, likely due to its unique protein composition, including the costains. The quantity of costa per cell suggests that further investigation is needed, potentially through synchronized cultures, to better understand the duplication process of the costa, particularly in cells with more than two costa. Future studies using ExM may provide deeper insights into the interactions between the protein components of the trichomonads and other cellular structures and organelles.

Estimated localization of each protein in the costa

In the attempt to estimate a more precise location of each of the three proteins in the costa, the position of gold-labeled particles was determined in 16 TEM images of each protein, taking into consideration their presence in the different bands of the costa. As seen in the graphic in Fig. 4, the costain-2 (11810) was more present in the electron-lucent bands but was also present in the electron-dense ones, with a proportion 1.4:1. There was also some labeling in the intermediary limit between both bands and also some labeling in the outer end of the costa. The labeling for the 32137 protein, in turn, was approximately two times more present in the electron-dense bands in comparison with the electron-lucent ones, with the proportion of electron-lucent to electron-dense being 1:2.09. The labeling also was present, in a less prominent way, in the region between the bands

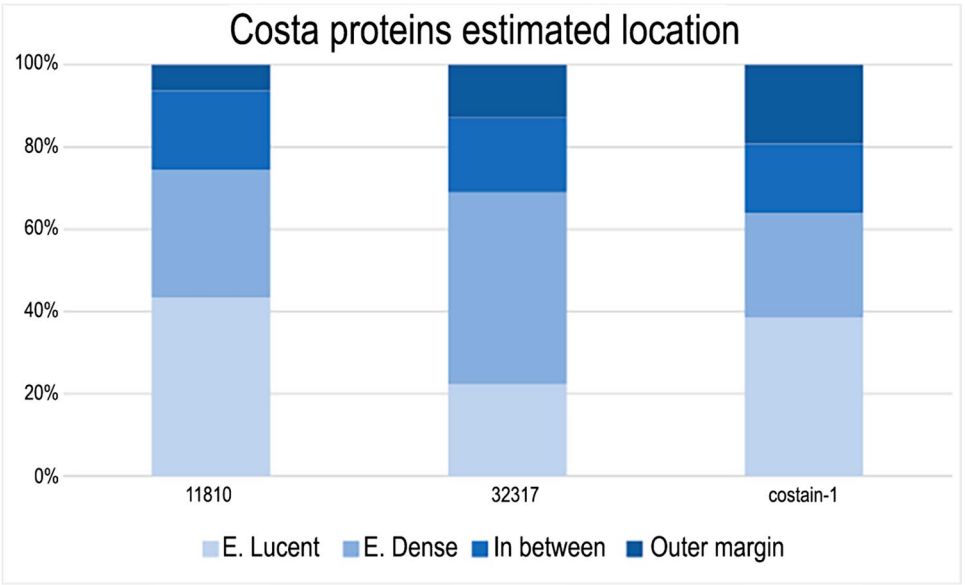

Fig. 4 Graphic showing the different distributions of the labeling of each protein in the costa according to the different striated patterns of the costa, subdivided into electron-lucent bands, electron-dense bands, between those two bands, and the outer corner of the costa. The results represent the total sum of labeling found at each analyzed location of the costa for each protein (costain-1 11810 and 32137) in EM images representative of three biologically independent experiments for each methodology used

Table 1 Identity matrix of the three costa proteins

Protein	Costain-1	Costain-2	Costain-3
Costain-1	100%	36%	36%
Costain-2	36%	100%	58%
Costain-3	36%	58%	100%

and also in the outer end of the costa. Finally, the labeling of the costain-1 showed great similarity with the 11810 labeling pattern, being more extensively present in the electron-lucent bands than the electron-dense bands (1.6:1). However, it also showed overall two times more labeling in the costa than the two other proteins, with an extensive presence also in the limits between bands and also at the outer end limits around the costa.

Sequence analysis and 3D protein modeling

The three costa proteins analyzed by this study were subjected to multiple sequence analysis, revealing that costain-1 shares an identity score of 36% with costains-2 and 3, while these share an identity score of 58% with each other (Table 1). This indicates that the studied proteins are very similar and likely homologous.

We then submitted all proteins to three different domain-identification servers, namely, SMART, InterPro, and CD-Search. The SMART server identified several coiled-coil domains for all three proteins, occasionally interspersed with predicted disordered domains or internal repeats (Fig. 5). InterPro also identified several coil domains and Centrosomal Protein 2 (Panther entry PTHR23159) as a domain hit for costains-1 and 2, while for costain-3, the domain identified was for Myosin Heavy Chain, Non-Muscle (Panther entry PTHR45615) (Supplementary Fig. 3). CD-Search identified the domain chromosome segregation protein SMC (structural maintenance of chromosomes) which is known to bind DNA and act in organizing and segregating chromosomes for partition (Supplementary Fig. 4).

Although there was no consensus between all three software, the common ground among all predictions was the highly helical content of the three proteins. Furthermore, all predicted domains are highly indicative of a cytoskeleton-related structural scaffold.

Finally, we submitted all sequences to structural prediction with AlphaFold3, which, expectedly, generated helical

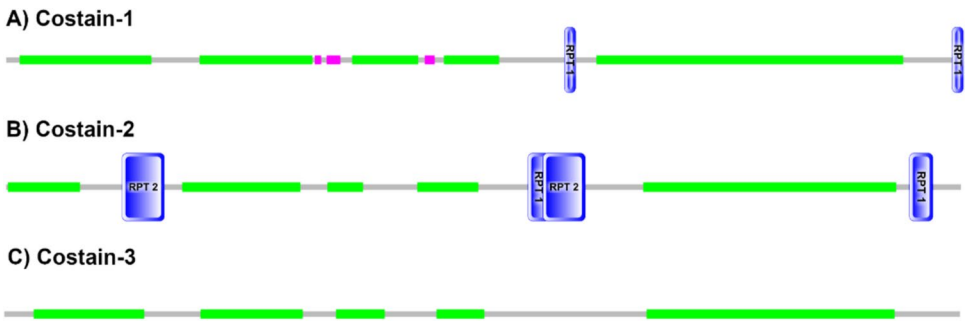

Fig. 5 Results obtained from the SMART server. Green spans are predicted coiled-coil regions, as detected by the COILS program. In pink are regions of low compositional complexity, as detected by the SEG program, and the blue rectangles are internal repeats, detected by the Prospero program

bundles with higher confidence (90 > plDDT > 70) on the helical spans and lower confidence on the disordered intervals (plDDT < 50). Costain-1 had an overall pTM score of 0.27 compared to 0.26 of costain-2 and 3 (Fig. 6). Interestingly, the pTM scores increased (to approximately 0.38) for all proteins when sequences were submitted as dimers (Fig. 7), but not as trimers, indicating that the functional scaffolds may be composed of dimeric proteins forming a parallel coiled-coil. It is important, however, to point out that these pTM and ipTM scores are still very low, indicating that the overall structure is significantly different from the AlphaFold3 output. We hypothesize that the scores are thus low due to the likely extended nature of these structural assemblies in detriment of the folded structure outputted by AlphaFold3.

Coiled-coil domains are very versatile and are involved in many cellular processes like membrane traffic (Gillingham and Sean 2003), regulation of transcription (Haque et al. 2022), protein–protein interactions (Adamczyk et al. 2021), among others. They are highly conserved in cytoskeletal and centrosomal proteins, e.g., intermediate filaments (Eldirany et al. 2021; Dang and Elmar 2022). Recently, it has been proposed that the assemble and strength of pericentriolar material is mediated by coiled-coil interactions between scaffold proteins in *C. elegans* (Rios et al. 2024), indicating its relevance in structural organization, which correlates to the structural maintenance of chromosomes domain found in costains by InterPro and CD-Search (Fig. 5). Interestingly, the proteome of *Tetratrichomonas gallinarum* cytoskeleton contains five proteins homologous to *Trichomonas vaginalis*' costa, and they also have long coiled-coil domains

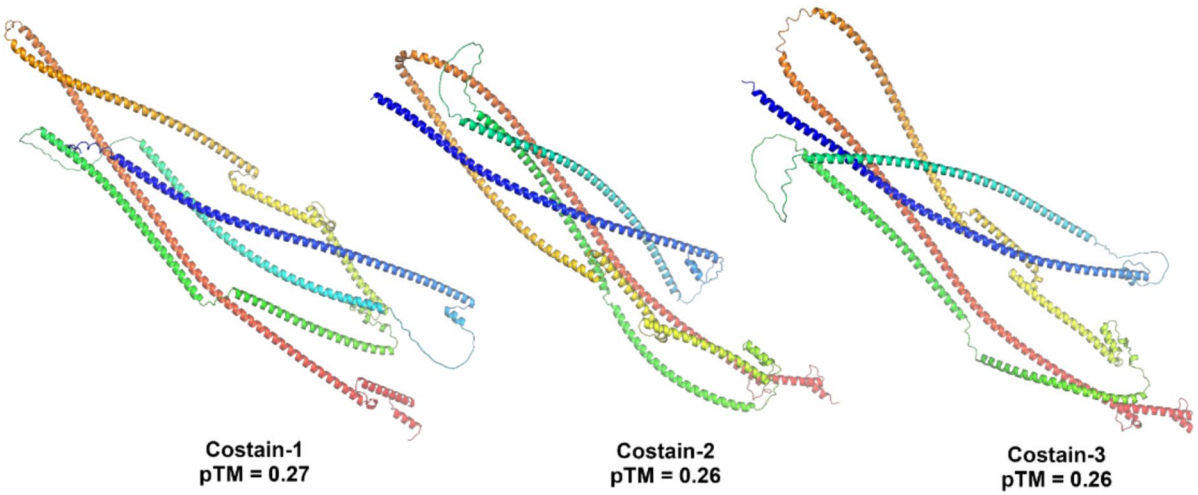

Fig. 6 AlphaFold 3 structural predictions of monomeric costain-1, 2, and 3 along with the predicted template modeling (pTM) score which measures the accuracy of the entire structure. A pTM score above 0.5 means the overall predicted fold for the complex might be similar to the true structure. All chains are colored from the N-terminal (blue) to the C-terminal (red)

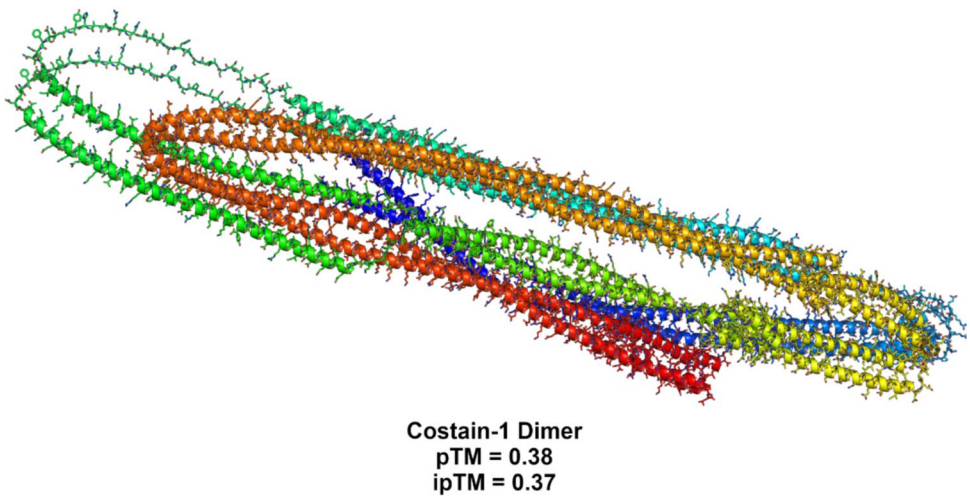

Fig. 7 AlphaFold 3 structural predictions of monomeric costain-1 dimer along with the predicted template modeling (pTM) and interface predicted template modeling (ipTM) scores which measure the accuracy of the entire structure. A pTM score above 0.5 means the overall predicted fold for the complex might be similar to the true structure. All chains are colored from the N-terminal (blue) to the C-terminal (red)

(Preisner et al. 2016). Preisner et al. suggest in this study that these filament-forming proteins share common structural properties with metazoan intermediate filaments, supporting our hypothesis that costain-1, 2, and 3 may have similar functions.

It is important to note that even being an early divergent eukaryote, the cytoskeleton of trichomonads and other eukaryote-like mammals still have a lot of common features, like the 3D model of the *T. vaginalis* tubulin dimer that is very similar to that of the pig brain (Noél et al. 2001), among other conserved aspects. However, it is still poorly explored the divergence, the common aspects, the origin, and the exact function of the rootlet structures usually associated with the basal bodies. These are present in a numerous type of eukaryotic cells and can become a useful and unique way to unravel relationships between these cells (Dingle and Larson 1981). In the last decades, these unique features of striated rootlets have been put to the side without answering some pivotal questions that were not possible to answer back then. Hopefully, it will be possible to use the new techniques and current knowledge to understand their origin, functions, and evolution in a better way.

Conclusions

In conclusion, we confirmed the presence of two new proteins in the costa of *T. foetus*: costain-2 (11810) and costain-3 (32137). Comparing the three identified proteins, we could note a slightly different localization in the striation pattern from the costa of each protein. This work also further characterizes these proteins as being highly α-helical and likely to assume a coiled-coil assembly. Finally, we predict them to have a structural role, as indicated by domains identified by the several prediction software (miosin, Centrosomal Protein 2, and chromosome segregation protein SMC) and provide the Alphafold3 models indicating a predicted template modeling of the proteins. The study of such unique proteins is important to better understand the costa structure and the relationship of these proteins and possibly determine a therapeutic future use as a drug target or its antigenic properties.

Supplementary Information The online version contains supplementary material available at https://doi.org/10.1007/s00436-025-08466-4.

Acknowledgements We thank Noemia Gonçalves for her expertise and aid in some experiments.

Author contribution Conceptualization: PTB, PHMT, WS; Methodology: PTB, PHMT; CRC; Software: PHMT; CRC; Resources, WS; Writing, original draft preparation: PTB; Writing, review and editing: PTB, WS, PHMT; Supervision, WS; Funding acquisition, WS. All authors have read and agreed to the published version of the manuscript.

Funding This work has been supported by Conselho Nacional de Desenvolvimento Científico e Tecnológico-CNPq, Fundação Carlos Chagas Filho de Amparo à Pesquisa do Estado do Rio de Janeiro (GRANT number E-26/200.956/2021), Funadesp, and Financiadora de Estudos e Projetos (FINEP).

Data availability No datasets were generated or analysed during the current study.

Declarations

Ethics approval Not applicable.

Consent to participate Not applicable.

Consent for publication Not applicable.

Conflict of interest The authors declare no competing interests.

Authorship I have read the Nature Portfolio journal policies on author responsibilities and submit this manuscript in accordance with those policies.

Third party material All of the material is owned by the authors and/or no permissions are required.

References

Abramson J, Adler J, Dunger J et al (2024) Accurate structure prediction of biomolecular interactions with AlphaFold 3. Nature 630:493–500. https://doi.org/10.1038/s41586-024-07487-w

Adamczyk ME, Lewicka R, Szatkowska H, Nieznanska J, Ludwiczak M, Jasiński S, Dunin-Horkawicz S et al (2021) Revealing biophysical properties of KfrA-type proteins as a novel class of cytoskeletal, coiled-coil plasmid-encoded proteins. BMC Microbiology 21:32. https://doi.org/10.1186/s12866-020-02079-w

Amos WB, Grimstone AV, Rothschild LJ (1979) Structure, protein composition and birefringence of the costa: a motile flagellar root fibre in the flagellate *Trichomonas*. J Cell Sci 35:139–164

Archibald JM (2015) Endosymbiosis and eukaryotic cell evolution. Curr Biol 25(19):R911–R921. https://doi.org/10.1016/j.cub.2015.07.055

Bandeira PT, de Souza W (2022) Costain 1 (ARM19800.1) - The first identified protein of the costa of the pathogenic protozoan Tritrichomonas foetus. Exp Parasitol 232:108177. https://doi.org/10.1016/j.exppara.2021.108177

Bandeira PT, das Neves Ortiz SF, Benchimol M, de Souza W (2023) Expansion microscopy of trichomonads. Exp Parasitol 255:108629. https://doi.org/10.1016/j.exppara.2023.108629

Bassey GB, Clarke AIL, Elhelu OK, Lee CM (2022) Trichomoniasis, a new look at a common but neglected STI in African descendance population in the United States and the Black Diaspora. A review of its incidence, research prioritization, and the resulting health disparities. J Natl Med Assoc 114:78–89. https://doi.org/10.1016/j.jnma.2021.12.007

Beatty NL, Forsyth CJ, Gilman RH et al (2022) Neglected testing for neglected tropical diseases at the CDC. Am J Trop Med Hyg 106:1571–1573. https://doi.org/10.4269/ajtmh.22-0222

Benchimol M (2004) Trichomonads under microscopy. Microsc Microanal 10:528–550. https://doi.org/10.1017/S1431927604040905

Benchimol M (2010) The mastigont system in trichomonads. Springer, Berlin, Heidelberg, pp 1–26

Benchimol M, Elias CA, de Souza W (1982) *Tritrichomonas foetus*: ultrastructural localization of basic proteins and carbohydrates. Exp Parasitol 54:135–144. https://doi.org/10.1016/0014-4894(82)90120-5

Dang H, Elmar S (2022) Emerging roles of centrosome cohesion. Open Biol 12(10):220229. https://doi.org/10.1098/rsob.220229

de Souza W (2024) Contribution of microscopy to a better understanding of the anatomy of pathogenic protists. Proc Natl Acad Sci U S A 121(17):e2321515121. https://doi.org/10.1073/pnas.2321515121

de Andrade Rosa I, Caruso MB, de Oliveira Santos E et al (2017) The costa of trichomonads: a complex macromolecular cytoskeleton structure made of uncommon proteins. Biology of the Cell 109:238–253. https://doi.org/10.1111/boc.201600050

Diamond LS (1957) The establishment of various trichomonads of animals and man in axenic cultures. J Parasitol 43. https://doi.org/10.2307/3274682

Dingle AD, Larson DE (1981) Structure and protein composition of the striated flagellar rootlets of some protists. BioSystems 14:345–358. https://doi.org/10.1016/0303-2647(81)90041-1

Dos Santos Pacheco N, Soldati-Favre D (2021) Coupling auxin-inducible degron system with ultrastructure expansion microscopy to accelerate the discovery of gene function in *Toxoplasma gondii*. In: Methods in Molecular Biology. Humana Press Inc., pp 121–137

Eldirany SA, Ivan BL, Minh H, Christopher GB (2021) Recent insight into intermediate filament structure. Curr Opin Cell Biol 68:132–143. https://doi.org/10.1016/j.ceb.2020.10.001

Eslahi AV, Olfatifar M, Abdoli A et al (2021) The neglected role of *Trichomonas tenax* in oral diseases: a systematic review and meta-analysis. Acta Parasitol 66:715–732. https://doi.org/10.1007/s11686-021-00340-4

Gillingham AK, Sean M (2003) Long coiled-coil proteins and membrane traffic. Biochem Biophys Acta 1641(2–3):71–85. https://doi.org/10.1016/s0167-4889(03)00088-0

Haque F, Freniere C, Ye Q, Mani N, Wilson-Kubalek EM, kU PI, Milligan RA, Subramanian RC (2022) Cytoskeletal regulation of a transcription factor by DNA mimicry via coiled-coil interactions. Nat Cell Biol 24(7):1088–1098. https://doi.org/10.1038/s41556-022-00935-7

Iriarte LS, Martinez CI, de Miguel N, Coceres VM (2023) *Tritrichomonas foetus* cell division involves DNA endoreplication and multiple fissions. Microbiology Spectrum 11. https://doi.org/10.1128/spectrum.03251-22

Laemmli UK (1970) Cleavage of structural proteins during the assembly of the head of bacteriophage T4. Nature 227(5259):680–685

Lassmann T (2020) Kalign 3: multiple sequence alignment of large datasets. Bioinformatics 36:1928–1929. https://doi.org/10.1093/bioinformatics/btz795

Letunic I, Khedkar S, Bork P (2021) SMART: recent updates, new developments and status in 2020. Nucleic Acids Res 49:D458–D460. https://doi.org/10.1093/nar/gkaa937

Matthew MA, Yang N, Ketzis J et al (2023) *Trichomonas tenax*: a neglected protozoan infection in the oral cavities of humans and dogs-a scoping review. Trop Med Infect Dis 8(1):60. https://doi.org/10.3390/tropicalmed8010060

Meites E (2013) Trichomoniasis: The "neglected" sexually transmitted disease. Infect Dis Clin North Am 27:755–764. https://doi.org/10.1016/j.idc.2013.06.003

Monteiro-Leal LH, Da Cunha-e-Silva NL, Benchimol M, De Souza W (1993) Isolation and biochemical characterization of the costa of *Tritrichomonas foetus*. Eur J Cell Biol 60:235–242

Muzny CA (2018) Why does *Trichomonas vaginalis* continue to be a "neglected" sexually transmitted infection? Clin Infect Dis 67:218–220. https://doi.org/10.1093/cid/ciy085

Noél C, Gerbod D, Nm F et al (2001) Tubulins in *Trichomonas vaginalis* : molecular characterization of α-tubulin genes, posttranslational modifications, and homology modeling of the tubulin dimer. J Eukaryot Microbiol 48:647–654. https://doi.org/10.1111/j.1550-7408.2001.tb00204.x

Okonechnikov K, Golosova O, Fursov M et al (2012) Unipro UGENE: a unified bioinformatics toolkit. Bioinformatics 28:1166–1167. https://doi.org/10.1093/bioinformatics/bts091

Paysan-Lafosse T, Blum M, Chuguransky S et al (2023) InterPro in 2022. Nucleic Acids Res 51:D418–D427. https://doi.org/10.1093/nar/gkac993

Preisner H, Eli LK, Gereon P, Kai S, Tal P, Sven BG (2016) The cytoskeleton of parabasalian parasites comprises proteins that share properties common to intermediate filament proteins. Protist 167(6):526–543. https://doi.org/10.1016/j.protis.2016.09.001

Rios MU, Małgorzata AB, Ryder BD, Gomes BF, Familiari NE, Yaguchi K, Amato M, Stachera WE, Joachimiak LA, Woodruff JB (2024) Multivalent coiled-coil interactions enable full-scale centrosome assembly and strength. J Cell Biol 223(4):e202306142. https://doi.org/10.1083/jcb.202306142

Secor WE, Meites E, Starr MC, Workowski KA (2014) Neglected parasitic infections in the United States: trichomoniasis. Am J Trop Med Hyg 90:800–804. https://doi.org/10.4269/ajtmh.13-0723

Sledge WE, Larson AD, Hart LT (1978) Costae of *Tritrichomonas foetus*: purification and chemical composition. Science 199:186–188. https://doi.org/10.1126/science.619450

Vidal JC, Alcantara CDL, de Souza W, Cunha-e-Silva NL (2016) Loss of the cytostomecytopharynx and endocytic ability are late events in Trypanosoma cruzi metacyclogenesis. J Struct Biol 196(3):319–328

Viscogliosi E, Brugerolle G (1993) Cytoskeleton in trichomonads: I. Immunological and biochemical comparative study of costal proteins in the genus *Tritrichomonas*. Eur J Protistol 29:160–170. https://doi.org/10.1016/S0932-4739(11)80269-5

Viscogliosi E, Brugerolle G (1994) Striated fibers in trichomonads: costa proteins represent a new class of proteins forming striated roots. Cell Motil Cytoskelet 29:82–93. https://doi.org/10.1002/cm.970290108

Wang J, Chitsaz F, Derbyshire MK et al (2023) The conserved domain database in 2023. Nucleic Acids Res 51:D384–D388. https://doi.org/10.1093/nar/gkac1096

Xu J, Zhang Y (2010) How significant is a protein structure similarity with TM-score = 0.5? Bioinformatics 26:889–895. https://doi.org/10.1093/bioinformatics/btq066

Zhang Y, Skolnick J (2004) Scoring function for automated assessment of protein structure template quality. Proteins: Structure. Funct Genet 57:702–710. https://doi.org/10.1002/prot.20264

The results/data/figures in this manuscript have not been published elsewhere, nor are they under consideration (from you or one of your contributing authors) by another publisher.